Heliyon 9 (2023) e16070

Contents lists available at ScienceDirect

Heliyon

journal homepage: www.cell.com/heliyon

Research article

MIL-100(Fe)-derived catalysts for CO_2 conversion via low- and high-temperature reverse water-gas shift reaction☆

Jesús Gandara Loe [a,*], Alejandro Pinzón Peña [a], Juan Luis Martin Espejo [a], Luis F. Bobadilla [a], Tomás Ramírez Reina [a,b], Laura Pastor-Pérez [a,b]

[a] Departamento de Química Inorgánica e Instituto de Ciencia de Materiales de Sevilla, Centro Mixto CSIC – Universidad de Sevilla, Av. Américo Vespucio 49, 41092, Sevilla, Spain
[b] Department of Chemical and Process Engineering, University of Surrey, Guildford, GU2 7XH, UK

ARTICLE INFO

Keywords:
CO_2 conversion
MOF-derived catalysts
Fe-based catalysts
RWGS reaction

ABSTRACT

Fe-derived catalysts were synthesized by the pyrolysis of MIL-100 (Fe) metal-organic framework (MOF) and evaluated in the reverse water-gas shift (RWGS) reaction. The addition of Rh as a dopant by in-situ incorporation during the synthesis and wet impregnation was also considered. Our characterization data showed that the main active phase was a mixture of α-Fe, Fe_3C, and Fe_3O_4 in all the catalysts evaluated. Additionally, small Rh loading leads to a decrease in the particle size in the active phase. Despite all three catalysts showing commendable CO selectivity levels, the C@Fe* catalyst showed the most promising performance at a temperature below 500 °C, attributed to the in-situ incorporation of Rh during the synthesis. Overall, this work showcases a strategy for designing novel Fe MOF-derived catalysts for RWGS reaction, opening new research opportunities for CO_2 utilization schemes.

1. Introduction

Climate change has not only forced modern society to develop new green technologies that minimize greenhouse gas emissions but also approaches to mitigate the consequence by reducing the main greenhouse gas impact. These approaches aim to reduce global temperature by 2 °C by 2050, achieving net zero carbon dioxide emissions globally [1,2]. In this sense, carbon conversion and reutilization are promising strategies to reduce the concentration of this gas via a circular technology. Amongst the different pathways for CO_2 upgrading, the reverse water-gas shift (RWGS) is a promising approach for the direct conversion of CO_2 into syngas (CO). The obtained CO can be further converted to valuable chemicals via the Fischer-Tropsch (FT) process [3]. Moreover, using H_2 in CO_2 conversion and utilization also motivates the development of hydrogen generation from renewable green sources.

$$H_2 + CO_2 \leftrightarrow CO + H_2O \quad \Delta H^{\circ}_{298K} = 41.2\ \mathrm{kJ/mol} \tag{1}$$

$$4H_2 + CO_2 \leftrightarrow CO_4 + 2H_2O \quad \Delta H^{\circ}_{298K} = -165\ \mathrm{kJ/mol} \tag{2}$$

The thermodynamic nature of the RWGS reaction favours the conversion at higher temperatures (Eq. (1)) i.e., >650 °C. However, at

☆ This article is a part of the "IMRC 22: Advanced Materials & Chemical Processes for CO2 Capture and Conversion".

* Corresponding author.
E-mail address: jgloe@us.es (J. Gandara Loe).

https://doi.org/10.1016/j.heliyon.2023.e16070
Received 9 February 2023; Received in revised form 7 April 2023; Accepted 4 May 2023
Available online 6 May 2023

lower temperatures, the equilibrium will be mainly displaced to the CO_2 methanation (Eq. (2)) due to its exothermic nature [4].

Therefore, shifting the equilibrium of the RWGS reaction out of the reference range by improving the catalytic activity is crucial for the efficiency and economics of the process. Furthermore, the FT process requires lower temperatures than those in RWGS [5] which confirms the aim of developing high-efficiency approaches. Hence, the design and tailoring of catalysts able to perform an improved activity at low temperatures enabling a combined RWGS-FT CO_2 conversion system, are highly appealing in a circular economy scenario.

Numerous catalysts, including noble metals and transition metals such as nickel, copper, and iron, have been studied in the RWGS reaction [6]. Among these metals, Fe-based catalysts have shown remarkable activity due to their stability in a wide range of temperatures where the main activity is related to the formation of $Fe^{3+} \leftrightarrow Fe^{2+}$ redox couple. However, the main drawback of these catalysts is the loss of activity due to the rapid formation of metallic iron (Fe^0) under a reducing atmosphere and high temperatures, which leads to a decrease in activity and poor selectivity [7]. Due to this, it is important to develop strategies that maintain Fe in oxide form, such as forming chemical bonds by adding small amounts of dopants to the iron oxide. For instance, Kharaji & Shariati studied the Mo–Fe/Al_2O_3 catalyst in the RWGS reaction probing the synergy between the two metals to improve the stability of the catalyst at higher temperatures [8]. Similarly, the addition of Co and Ni into Fe-based catalysts has shown a drastic improvement in the CO_2 yield compared to the undoped catalyst [9].

The addition of noble metals such as Pd [10], Pt [11], and Rh [12] in catalyst systems for the RWGS reaction has been widely studied due to their high hydrogenation capacity and CO selectivity. In this sense, it has been reported that small amounts of noble metals such as Rh works as dopant modifying not only the textural properties but also the chemical and electronic properties of the active phase [12,13]. For instance, Gogate & Davis studied the CO and CO_2 hydrogenation over supported Rh–Fe catalysts showing the boosting not only in the CO selectivity but also in the formation of bigger molecules such as ethanol [12].

Metal-organic frameworks (MOFs) are crystalline porous materials formed by the ensemble of organic linkers and metal ions or clusters [14]. Due to their versatility, MOFs can be tailored and tuned for desired applications. MOFs have been studied and applied in different applications, such as gas adsorption/separation, drug delivery, sensors, and water treatment [15]. Unfortunately, the use of these materials in gas-phase reactions such as RWGS is limited due to the reaction conditions, i.e. high temperatures. Nevertheless, several studies have shown that the pyrolysis of MOFs leads to carbonaceous materials with a highly dispersed active phase which can be suitable for a gas reaction such as RWGS [16–18]. For instance, M. Ronda-Lloret et al. studied the use of Cu-BTC as active phase precursor in the development of RWGS reaction by impregnation of the MOF into CeOx precursor and further pyrolysis. It was observed that the MOF-derived catalyst showed a better performance compared with similar catalyst systems synthesized by a different method [19].

MIL-100 (Fe) (MIL = *Matériaux de l'Institut Lavoisier*) is a mesoporous MOF formed by Fe (III) metal cluster and 1,3,5-tricarboxilate (BTC) linkers forming a 3D framework with cages of 2.5 nm and 2.9 nm size (Scheme 1) [20]. Additionally, MIL-100 (Fe) presents open metal sites (OMSs) that favour the adsorption of guest molecules. Commonly, MIL-100 (Fe) has been synthesized by solvothermal method using HF as a reagent [21]. However, recently it has been reported the green synthesis of MIL-100 (Fe) under HF-free conditions.

Based on these premises, this research aims to synthesize MOF-derived catalysts by the pyrolysis of MIL-100 (Fe) evaluating the effect of adding small amounts of Rh as a dopant in the catalytic performance in the RWGS reaction. Such proof-of-concept can unlock the potential of MOF-derived catalysts for their direct application in CO_2 valorization reactions.

2. Experimental methodology and techniques

2.1. Chemical reagents

In this study, MOF-based catalysts precursors were synthesized using trimesic acid [$C_6H_3(CO_2H)_3$] 95%, iron nitrate [$Fe(NO_3)_3 \cdot 9H_2O$] 99%, ethanol (>99.5%), and Rhodium Chloride [$RhCl_3$:xH_2O] 38% Rh.

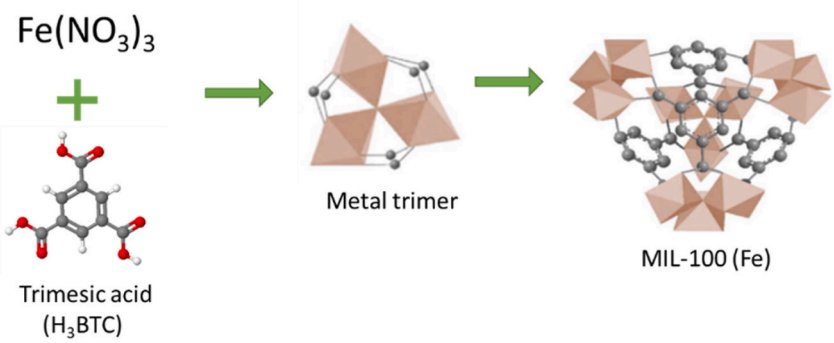

Scheme 1. Schematic synthesis of MIL-100 (Fe) [22].

2.2. Synthesis of the catalysts

Catalysts precursors were synthesized by solvothermal method adapted from the literature to incorporate Rh in the framework [20]. Firstly, MIL-100 (Fe) was synthesized using an HF-free green synthesis by mixing 1.89 g of trimesic acid (9 mmol) and 4.04 g (10 mmol) of $Fe(NO_3)_3{\cdot}9H_2O$ in 6 mL of distilled water. After that, the solution was kept under reflux at 95 °C for 12 h. The resulting powder was collected by filtration and washed in a mixture of ethanol: water 1:1 at 70 °C for 24 h. Finally, the MIL-100(Fe) was activated in a vacuum oven at 120 °C for 10 h.

Rh was incorporated in the MIL-100 using *(1)* in-situ incorporation during solvothermal synthesis and *(2)* by impregnation of the activated MIL-100 (Fe). The in-situ synthesized bimetallic MOF (*MIL100-FeRh**) was synthesized by the incorporation of 1.5 wt% of Rh using $RhCl_3{:}xH_2O$ (Fe/Rh ratio of 98.5:1.5) into the above-described synthesis. After this step, the material was purified and activated using the same procedure. Finally, the Rh-impregnated MIL-100 (*MIL100-FeRh*$^+$) was synthesized by impregnation in water of 1.5 wt% of Rh using $xRhCl_3{\bullet}H_2O$ (Fe/Rh ratio of 98.5:1.5) in the activated MIL-100 (Fe). After the impregnation, the sample was dried using a rotary pump and reactivated for an extra 10 h at 120 °C. Finally, the 3 materials synthesized were pyrolyzed at 800 °C using a tubular furnace under an inert gas atmosphere (50 mL/min N_2) and a heating ramp of 5 °C/min for 4 h. For clarity, the catalysts were named as C@Fe for the catalyst obtained from MIL-100(Fe), C@FeRh* for the catalyst obtained from MIL100-FeRh* and C@FeRh$^+$ for the catalyst obtained from MIL100-FeRh$^+$.

2.3. X-ray diffraction measurements

X-ray diffraction patterns of the catalysts precursors and the catalysts were collected using X'Pert Pro PANalytical equipment equipped with CuKα source (40 mA, 45 kV) and X'Celerator detector in the range of $2\theta = 5\text{-}90°$ using a step size and time of 0.05° and 300 s, respectively.

2.4. Nitrogen isotherms at −196 °C

The Nitrogen isotherms of the catalyst were collected using a volumetric equipment brand Micromeritics model Tristar II. Prior to the measurements, the samples were outgassed at 120 °C for 6 h under a dynamic vacuum. The surface area was calculated using the BET model and the pore volume using the BJH model.

2.4.1. Transmission electron microscopy

The morphology and metal dispersion was evaluated using a high-resolution transmission electron microscope JEOL 2100Plus (200 kV) equipped with a LaB6 filament and resolution of 0.14 and 0.23 nm between point and lines, respectively. Additionally, the microscope has coupled equipment for the analysis of the X-ray dispersion energy and a CCD camera.

2.5. Catalytic activity

The catalytic activity of the samples was evaluated using a steel stillness continue flow reactor system commercially available by PID. In a typical experiment, 0.2 g of the catalyst was mixed with the required amount of SiC to build a homogenous bed of 1 cm^3 and placed in the middle part of the stainless steel reactor. Firstly, the catalyst was pre-reduced at 700 °C for 1 h under a flow of 100 mL/min H_2/N_2 (50:50). Once the system reached room temperature, the catalyst was exposed to an inlet stream of 100 mL/min of gas mixture flow (50% N_2, 40% H_2 and 10% CO_2). The RWGS reaction was screened in the temperature range of 200–700 °C using a heating rate of 10 °C/min and keeping isothermal in each step for 1 h. All the experiments were performed at atmospheric pressure and weight hourly space velocity (WHSV) of 30 000 mL g^{-1} h^{-1}. The outlet stream was analyzed using a micro-GC Varian 4900 equipped with Porapak Q and MS-5A columns. The CO_2 conversion (Eq. (3)) and the CO (Eq. (4)) and CH_4 (Eq. (5)) selectivity were calculated using the following equations:

$$X_{CO_2}(\%) = \frac{F^{in}_{CO_2} - F^{out}_{CO_2}}{F^{in}_{CO_2}} \times 100 \tag{3}$$

$$S_{CH4}(\%) = \frac{F^{out}_{CH_4}}{F^{in}_{CO_2} - F^{out}_{CO_2}} \times 100 \tag{4}$$

$$S_{CO}(\%) = \frac{F^{out}_{CO}}{F^{in}_{CO_2} - F^{out}_{CO_2}} \times 100 \tag{5}$$

Where.

$F^{in}_{CO_2}$ = Molar Flow of CO_2 in the inlet stream
$F^{out}_{CO_2}$ = Molar Flow of CO_2 in the outlet stream
F^{out}_{CO} = Molar Flow of CO in the outlet stream

$F_{CH_4}^{out}$ = Molar Flow of CH_4 in the outlet stream

Additionally, the theoretical thermodynamic equilibrium for CO_2 conversion in the analyzed temperature range and flow conditions was calculated using ChemCad software (Soave-Redlich-Kwong equation of state) in order to provide an in-depth overview of the experimental results.

3. Results and discussion

XRD measurements were performed in the MIL-100 (Fe) and in the bimetallic MIL-100 (Fe, Rh) synthesized by HF-free method to evaluate their crystallinity. As it is observed in Fig. 1, the three catalyst precursor show similar diffraction peaks in good agreement with the simulated pattern obtained from the literature [23]. The lower crystallinity observed in the synthesized materials has been widely described as a consequence of the absence of HF in the synthesis. However, it has been reported that this difference in crystallinity does not have a considerable impact on the textural properties and, most importantly, on the final catalysts [20,24,25].

The XRD patterns of the C@Fe, C@FeRh* and C@FeRh^{+} catalysts are shown in Fig. 2. After the MOFs pyrolysis, it is observed in the three patterns characteristic peaks of α-Fe at 44.5°, 65° and 82° (JCPDS no. 06–0696), also a small amount of magnetite (Fe_3O_4 JCPDS no. 19–0692) with peaks at 35.6°, 43.2° and 52° and iron carbide species (Fe_3C JCDPS no. 35–0772) with peaks at 43.7° and 44.5°. However, no diffraction peaks from Rh are observed C@FeRh^{+} and C@FeRh* XRD pattern due to the low amount of Rh loaded and, most importantly, due to the high metal dispersion in the carbonaceous support. As confirmed by the XRD analysis, the pyrolysis conditions favour the formation of α-Fe species in the coexistence of small amounts of Fe_3O_4 and Fe_3C species responsible for the catalytic activity in Fe-derived materials [26].

Nitrogen adsorption-desorption measurements were performed at −196 °C in the three catalysts to evaluate the textural properties. As it has been widely reported in the literature, MIL-100 (Fe) is a porous material formed by narrow mesoporous cages of 2.5 nm and 2.9 nm and an average BET surface area of 1836 m^2/g [20]. Nevertheless, after the MOF precursors pyrolysis, the isotherm of the catalyst shows a mainly mesoporous material (Fig. 3) with an isotherm type IV and H3 hysteresis loop. As is observed in Table 1, the catalyst shows a low surface area due to the pyrolysis of the framework, which leads to a carbonaceous matrix with metals dispersed on the surface.

The C@FeRh* catalyst obtained from the pyrolysis of MIL100-FeRh* shows a slight increase in the surface area, probably due to the incorporation of Rh atoms in the framework metal nodes rather than the Rh impregnation on the MOF surface (MIL-100-FeRh^{+}) which ensures a Fe–Rh atomic contact boosting the dispersion of the Fe. The effect of Rh into the dispersion of transition metals-based catalysts has been widely reported in the literature [27,28].

Fig. 4 shows the TEM images of the monometallic catalyst (C@Fe) and the two bimetallic catalysts (C@FeRh^{+} and C@FeRh*). Fe particles of ca. 80 nm (Fig. 4a) dispersed in the carbonaceous matrix are observed in the monometallic catalyst, while the incorporation of Rh has an important effect in decreasing the particle size. For both bimetallic catalysts, it is observed a particle size heterogeneity with particles of ca. 50 nm and small particles of 2–5 nm (Fig. 4b and c). It has been reported in the literature that small amounts of noble metals not only work to boost the CO selectivity but also enhance the dispersion of the active phase in the catalyst [27,28].

The catalytic activity of the synthesized catalyst was evaluated in the RWGS reaction using an H_2:CO_2 ratio of 4:1 to force the catalytic system to operate in extreme conditions where the selectivity of methane is favoured in order to evidence the capability of the catalyst to work under a wide range of conditions. As observed in Fig. 5, the monometallic and the two bimetallic catalysts present a similar performance in terms of CO_2 conversion behaviour below 300 °C. However, with the increase of the temperature, the bimetallic C@Fe* catalyst shows an improved catalytic activity in terms of CO_2 conversion attributed to the smaller particle size and also to the increase of the surface area, which is in good agreement with the results discussed above. On the other side, the bimetallic catalyst

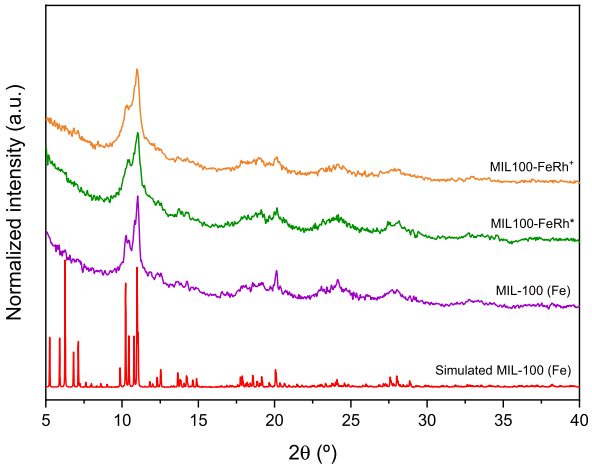

Fig. 1. Powder XRD pattern of the catalyst precursors and the simulated pattern of MIL-100 (Fe) [23].

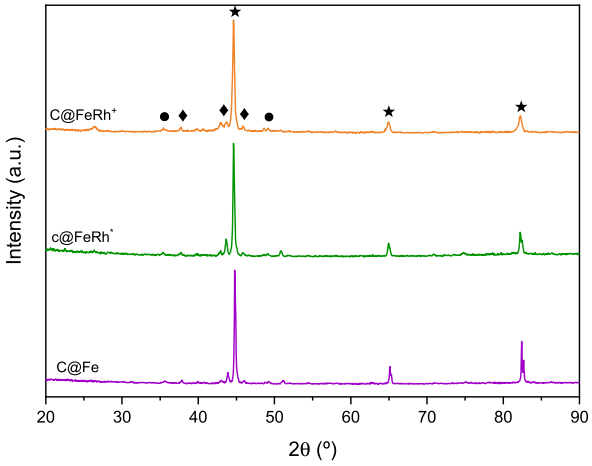

Fig. 2. XRD pattern of the as-synthesized catalysts (★ α-Fe, ◆ Fe_3C and ● Fe_3O_4).

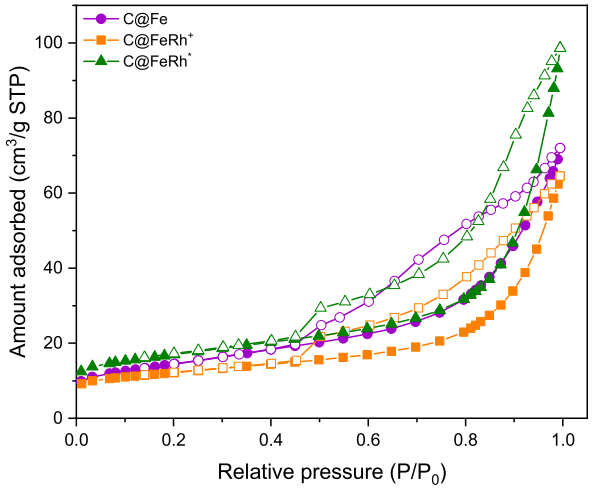

Fig. 3. Nitrogen adsorption-desorption isotherms at −196 °C on the synthesized catalysts. (Filled symbols = adsorption and empty symbols = desorption).

Table 1
Textural properties of the catalysts.

Sample	S_{BET} (m^2/g)	Pore volume (cm^3/g)	Average pore size (Å)
C@Fe	51	0.10	77.11
C@FeRh*	59	0.13	85.31
C@FeRh$^+$	42	0.08	79.22

obtained from the pyrolysis of the Rh wet-impregnated MIL-100 (Fe) shows a decrease in the CO_2 conversion compared to the other two mentioned catalysts, which can be attributed to the encapsulation of the active phase deposited in the framework cages during the pyrolysis of the MOF [29,30].

Fig. 6 shows the methane selectivity in the temperature screening from 200 °C to 700 °C in all three catalysts. It is observed in the evaluated catalysts a low methane selectivity showing maximum selectivity at 450 °C. However, in the case of the monometallic catalyst, the selectivity increases up to 8%, while this behaviour is completely suppressed in the C@Fe* catalyst. This low affinity for the CO_2 methanation using Fe-based catalysts has been explained due to the dynamic nature of the carburization-oxidation governed by the thermodynamic equilibrium to CO [31].

Finally, Fig. 7 shows the CO selectivity for the catalysts in the evaluated temperature range. In all cases, the CO selectivity is close to 100% at higher temperatures (i.e., >500 °C). However, at low temperatures, the C@Fe* catalyst shows a booster compared to the other two evaluated catalysts, which agrees with the results discussed above. Additionally, Table 2 compares the catalytic activity in the

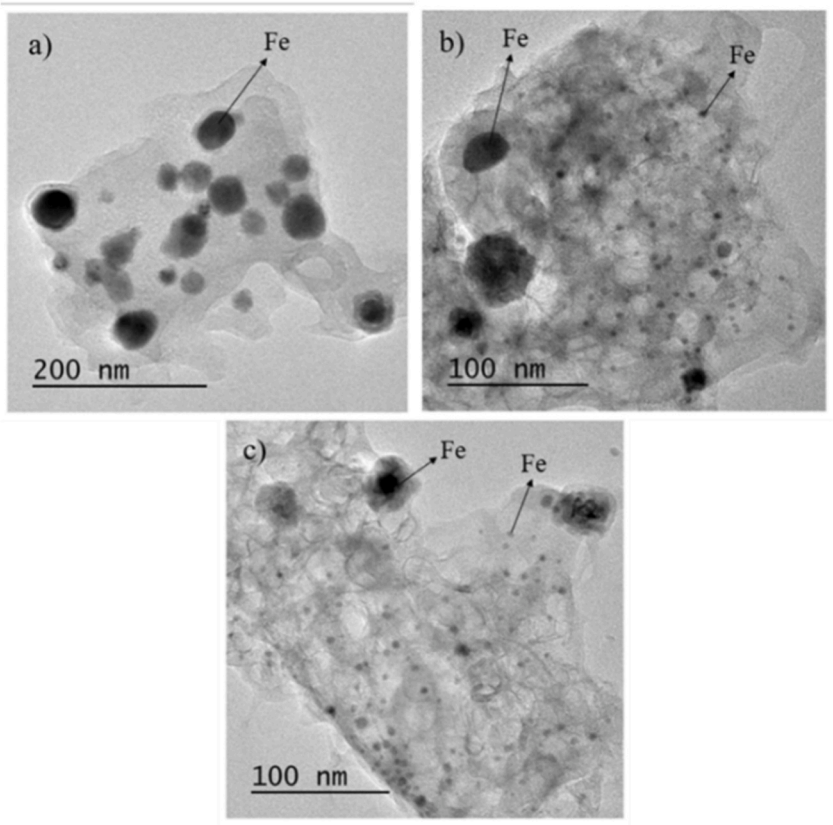

Fig. 4. TEM images of (a) C@Fe, (b) C@FeRh^{+} and C@FeRh*

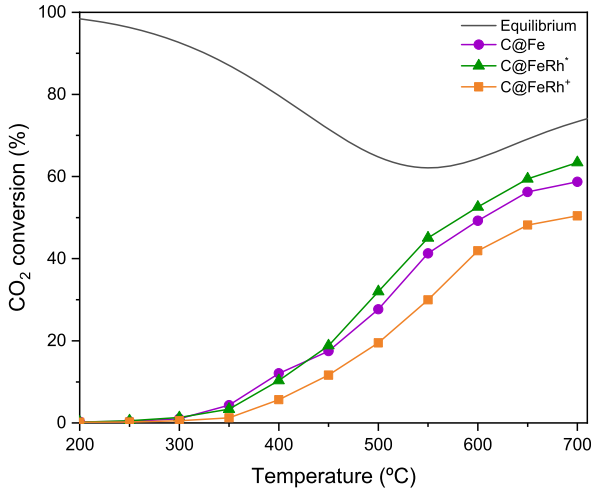

Fig. 5. CO_2 conversion in the RWGS temperature screening of the catalysts and equilibrium at WHSV = 30 000 mg L^{-1} h^{-1}, H_2/CO_2 = 4:1 and atmospheric pressure.

RWGS reaction of the C@Fe* catalyst with some examples extracted from the literature. Although, CO_2 methanation is thermodynamically favoured at low temperatures challenging the CO selectivity in this temperature range, the C@Fe* catalyst offers a selectivity of 100% and CO_2 conversion of 33% at 500 °C, which makes it a promising catalyst for low- and high-temperature RWGS.

Overall, the results presented in this section demonstrate the potential and versatility of this catalytic system to operate in both low- and high-RWGS reaction conditions. Nevertheless, it is important to continue exploring different factors that affect the performance of these catalysts, such as their reusability and regenerability. The development of highly efficient and reusable catalysts is a crucial step

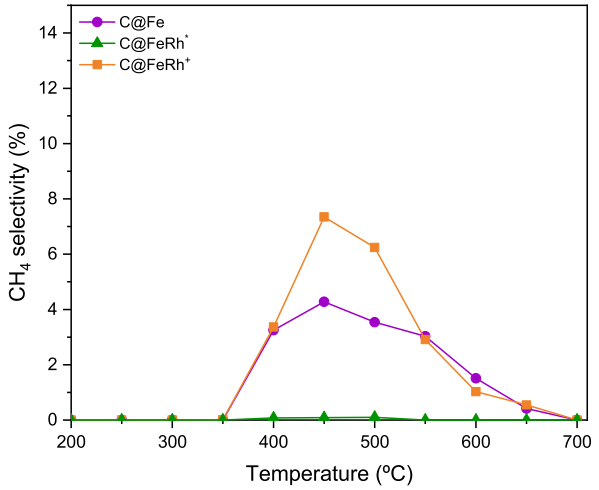

Fig. 6. CH_4 selectivity in the RWGS temperature screening of the catalysts at WHSV = 30 000 mg L^{-1} h^{-1}, H_2/CO_2 = 4:1 and atmospheric pressure.

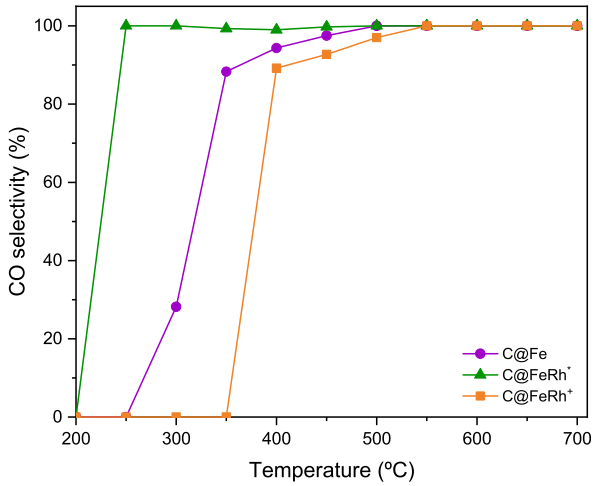

Fig. 7. CO selectivity in the RWGS temperature screening of the catalysts at WHSV = 30 000 mg L^{-1} h^{-1}, H_2/CO_2 = 4:1 and atmospheric pressure.

Table 2
Comparison of the catalytic activity of the studied catalysts versus benchmark systems from the literature.

Catalyst	Temperature (°C)	X_{CO2} (%)	S_{CH4} (%)	S_{CO} (%)	WHSV (mL•g^{-1}•h^{-1})	Ref.
C@FeRh* (1.5 wt%)	500	37	0	100	30 000	This work
Pt/TiO_2 (1 wt%)[a]	400	21	4	92	–	[32]
FexC	500	39	3	60	–	[33]
FexC-im	500	38	2	62	–	[33]
Ni-CeO_2-CP[a] (1 wt%)	500	29	22	79	60 000	[34]
Ce-HT	500	10	–	94	60 000	[35]
Cu/β-Mo_2C (1 wt%)	550	35	–	99	30 000	[36]
Cu/ZnO/Al_2O_3 (40 wt%)	500	18	–	100	90 000	[37]
Co-CE	400	35	37	65	–	[38]
Ni–MgO[a] (15 wt%)	500	25	40	60	–	[39]
CsFe/Al_2O_3 (2.5 wt%)	500	52	5	82	12 000	[40]

[a] H_2:CO_2 = 1:1.

towards more sustainable chemical processes. Therefore, investigating and optimizing the reusability and regenerability of these catalysts should be a focus of future research in the field.

Finally, the XRD of the spent catalysts were evaluated to obtain information related to the effect of the Rh in the Fe active phase after the catalytic screening. As observed in Fig. 8, the three spent catalysts present similar diffraction peaks, which correspond to the

α-Fe phase (JCPDS no. 06–0696). Nevertheless, the diffraction peaks corresponding to Fe_3O_4 and Fe_3C phases disappear after the catalytic test due to their reduction to Fe, which has been reported also as an active phase for the process [26]. Such catalyst dynamics during reaction merits further perhaps under operando conditions to gather further mechanistic information which is beyond this proof-of-concept work. In any case, herein we validate the application of MOFs-derived Fe-based catalysts for the RWGS and the positive impact of Rh as dopant leading to commendable performances in the full temperature range.

4. Conclusions

Fe-MOF-derived catalysts were obtained by pyrolysis of MOF precursors and evaluated in the RWGS reaction. Furthermore, the addition of Rh by two different strategies was also evaluated. After pyrolysis, a carbonaceous material with active phases of Fe_3O_4, Fe_3C and Fe^0 was obtained. The addition of Rh into the Fe-MOF precursor modified not only the textural properties of the catalyst but also the catalytic activity due to the decrease of the particle size of the active phase. For instance, the addition of Rh via in-situ (C@FeRh*) increased the CO_2 conversion to up to 37% but also boosted the CO selectivity by 100% at 500 °C, and most importantly, suppressing almost completely the CH_4 selectivity at low temperatures. In this sense, our MOF-derived catalysts stand as promising materials for the RWGS in low- and high-temperature ranges due to their catalytic activity when compared with benchmark catalysts.

All in all, our work showcases the successful the application of MOFs-derived Fe-based catalysts for the RWGS serving as new example of MOFs versatility for green chemistry applications and very importantly opening new research avenues in the urgent field of CO_2 valorization.

Author contribution statement

Jesus Gandara-Loe: Analyzed and interpreted the data; Wrote the paper.

Alejandro Pinzón-Peña, Juan Luis Martin Espejo: Performed the experiments.

Luis Bobadilla: Contributed reagents, materials, analysis tools or data; Wrote the paper.

Tomás Ramírez Reina, Laura Pastor-Pérez: Conceived and designed the experiments; Contributed reagents, materials, analysis tools or data; Wrote the paper.

Data availability statement

Data included in article/supplementary material/referenced in article.

Funding

The authors would like to acknowledge financial support from grants PID2019-108502 R J-I00 and IJC2019-040560-I, both funded by MCIN/AEI/10.13 039/501 100 011 033 and by ESF Investing in your future. This research was also partially funded by the Junta de Andalucia PAIDI2020 programme through the CLEVER-BIO project P20_00667.

Declaration of competing interest

The authors declare that they have no known competing financial interests or personal relationships that could have appeared to

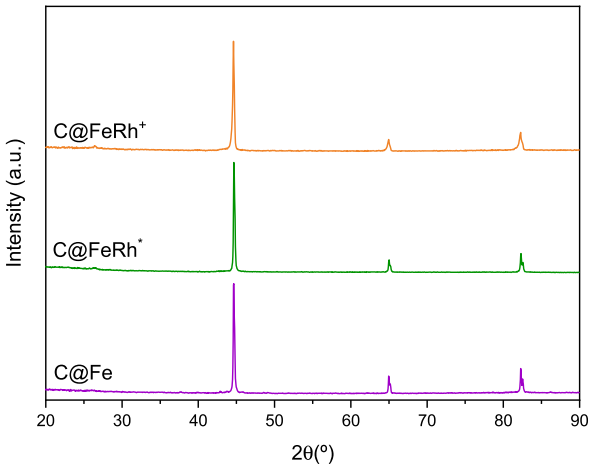

Fig. 8. XRD pattern of the spent catalysts.

influence the work reported in this paper

References

[1] A. Garcia, J. Monsalve-Serrano, R. Lago Sari, S. Tripathi, Pathways to achieve future CO2 emission reduction targets for bus transit networks, Energy 244 (2022), 123177, https://doi.org/10.1016/j.energy.2022.123177.

[2] J. Krause, C. Thiel, D. Tsokolis, Z. Samaras, C. Rota, A. Ward, P. Prenninger, T. Coosemans, S. Neugebauer, W. Verhoeve, EU road vehicle energy consumption and CO2 emissions by 2050 – expert-based scenarios, Energy Pol. 138 (2020), 111224, https://doi.org/10.1016/j.enpol.2019.111224.

[3] M. Gonzalez-Castano, B. Dorneanu, H. Arellano-Garcia, The reverse water gas shift reaction: a process systems engineering perspective, React Chem Eng 6 (2021) 954–976, https://doi.org/10.1039/D0RE00478B.

[4] K. Stangeland, D. Kalai, H. Li, Z. Yu, CO 2 methanation: the effect of catalysts and reaction conditions, Energy Proc. 105 (2017) 2022–2027, https://doi.org/10.1016/j.egypro.2017.03.577.

[5] X. Shen, Q. Meng, M. Dong, J. Xiang, S. Li, H. Liu, B. Han, Low-temperature reverse water–gas shift process and transformation of renewable carbon resources to value-added chemicals, ChemSusChem 12 (2019) 5149–5156, https://doi.org/10.1002/cssc.201902404.

[6] M. Zhu, Q. Ge, X. Zhu, Catalytic reduction of CO2 to CO via reverse water gas shift reaction: recent advances in the design of active and selective supported metal catalysts, Trans. Tianjin Univ. 26 (2020) 172–187, https://doi.org/10.1007/s12209-020-00246-8.

[7] S.-W. Park, O.-S. Joo, K.-D. Jung, H. Kim, S.-H. Han, ZnO/Cr2O3 catalyst for reverse-water-gas-shift reaction of CAMERE process, Kor. J. Chem. Eng. 17 (2000) 719–722, https://doi.org/10.1007/BF02699123.

[8] A.G. Kharaji, A. Shariati, Performance comparison of two newly developed bimetallic (X-Mo/Al2O3, X=Fe or Co) catalysts for reverse water gas shift reaction, China Pet. Process. Petrochem. Technol. 18 (2016) 51–58.

[9] S. Sengupta, A. Jha, P. Shende, R. Maskara, A.K. Das, Catalytic performance of Co and Ni doped Fe-based catalysts for the hydrogenation of CO2 to CO via reverse water-gas shift reaction, J. Environ. Chem. Eng. 7 (2019), 102911, https://doi.org/10.1016/j.jece.2019.102911.

[10] D.J. Pettigrew, D.L. Trimm, N.W. Cant, The effects of rare earth oxides on the reverse water-gas shift reaction on palladium/alumina, Catal. Lett. 28 (1994) 313–319, https://doi.org/10.1007/BF00806061.

[11] M.D. Porosoff, X. Yang, J.A. Boscoboinik, J.G. Chen, Molybdenum carbide as alternative catalysts to precious metals for highly selective reduction of CO $_2$ to CO, Angew. Chem. Int. Ed. 53 (2014) 6705–6709, https://doi.org/10.1002/anie.201404109.

[12] M.R. Gogate, R.J. Davis, Comparative study of CO and CO2 hydrogenation over supported Rh–Fe catalysts, Catal. Commun. 11 (2010) 901–906, https://doi.org/10.1016/j.catcom.2010.03.020.

[13] B. Yan, Q. Wu, J. Cen, J. Timoshenko, A.I. Frenkel, D. Su, X. Chen, J.B. Parise, E. Stach, A. Orlov, et al., Highly active subnanometer Rh clusters derived from Rh-doped SrTiO3 for CO2 reduction, Appl. Catal., B 237 (2018) 1003–1011, https://doi.org/10.1016/j.apcatb.2018.06.074.

[14] H.-C. Zhou, Joe, S. Kitagawa, Metal–organic frameworks (MOFs), Chem. Soc. Rev. 43 (2014) 5415–5418, https://doi.org/10.1039/C4CS90059F.

[15] H.-C. Zhou, J.R. Long, O.M. Yaghi, Introduction to metal–organic frameworks, Chem. Rev. 112 (2012) 673–674, https://doi.org/10.1021/cr300014x.

[16] Q. Wang, D. Astruc, State of the art and prospects in metal–organic framework (MOF)-Based and MOF-derived nanocatalysis, Chem. Rev. 120 (2020) 1438–1511, https://doi.org/10.1021/acs.chemrev.9b00223.

[17] A. Han, B. Wang, A. Kumar, Y. Qin, J. Jin, X. Wang, C. Yang, B. Dong, Y. Jia, J. Liu, et al., Recent advances for MOF-derived carbon-supported single-atom catalysts, Small Methods 3 (2019), 1800471, https://doi.org/10.1002/smtd.201800471.

[18] K. Shen, X. Chen, J. Chen, Y. Li, Development of MOF-derived carbon-based nanomaterials for efficient catalysis, ACS Catal. 6 (2016) 5887–5903, https://doi.org/10.1021/acscatal.6b01222.

[19] M. Ronda-Lloret, S. Rico-Frances, A. Sepulveda-Escribano, E.v. Ramos-Fernandez, CuOx/CeO2 catalyst derived from metal organic framework for reverse water-gas shift reaction, Appl. Catal. Gen. 562 (2018) 28–36, https://doi.org/10.1016/j.apcata.2018.05.024.

[20] F. Zhang, J. Shi, Y. Jin, Y. Fu, Y. Zhong, W. Zhu, Facile synthesis of MIL-100(Fe) under HF-free conditions and its application in the acetalization of aldehydes with diols, Chem. Eng. J. 259 (2015) 183–190, https://doi.org/10.1016/j.cej.2014.07.119.

[21] P. Kusgens, M. Rose, I. Senkovska, H. Frode, A. Henschel, S. Siegle, S. Kaskel, Characterization of metal-organic frameworks by water adsorption, Microporous Mesoporous Mater. 120 (2009) 325–330, https://doi.org/10.1016/j.micromeso.2008.11.020.

[22] N.M. Mahmoodi, J. Abdi, M. Oveisi, M. Alinia Asli, M. Vossoughi, Metal-organic framework (MIL-100 (Fe)): synthesis, detailed photocatalytic dye degradation ability in colored textile wastewater and recycling, Mater. Res. Bull. 100 (2018) 357–366, https://doi.org/10.1016/j.materresbull.2017.12.033.

[23] P. Horcajada, S. Surble, C. Serre, D.-Y. Hong, Y.-K. Seo, J.-S. Chang, J.-M. Greneche, I. Margiolaki, G. Ferey, Synthesis and catalytic properties of MIL-100(Fe), an iron(<scp>iii</Scp>) carboxylate with large pores, Chem. Commun. (2007) 2820–2822, https://doi.org/10.1039/B704325B.

[24] S. Duan, J. Li, X. Liu, Y. Wang, S. Zeng, D. Shao, T. Hayat, HF-free synthesis of nanoscale metal–organic framework NMIL-100(Fe) as an efficient dye adsorbent, ACS Sustain. Chem. Eng. 4 (2016) 3368–3378, https://doi.org/10.1021/acssuschemeng.6b00434.

[25] N.E. Elharony, I.E.T. el Sayed, A.G. Al-Sehemi, A.A. Al-Ghamdi, A.S. Abou-Elyazed, Facile synthesis of iron-based MOFs MIL-100(Fe) as heterogeneous catalyst in kabachnick reaction, Catalysts 11 (2021) 1451, https://doi.org/10.3390/catal11121451.

[26] J. Liu, A. Zhang, M. Liu, S. Hu, F. Ding, C. Song, X. Guo, Fe-MOF-Derived highly active catalysts for carbon dioxide hydrogenation to valuable hydrocarbons, J. CO2 Util. 21 (2017) 100–107, https://doi.org/10.1016/j.jcou.2017.06.011.

[27] W.-J. Cai, L.-P. Qian, B. Yue, H.-Y. He, Rh doping effect on coking resistance of Ni/SBA-15 catalysts in dry reforming of methane, Chin. Chem. Lett. 25 (2014) 1411–1415, https://doi.org/10.1016/j.cclet.2014.06.016.

[28] D. Li, T. Shishido, Y. Oumi, T. Sano, K. Takehira, Self-activation and self-regenerative activity of trace Rh-doped Ni/Mg(Al)O catalysts in steam reforming of methane, Appl. Catal. Gen. 332 (2007) 98–109, https://doi.org/10.1016/j.apcata.2007.08.008.

[29] J. Grams, A.M. Ruppert, Catalyst stability—bottleneck of efficient catalytic pyrolysis, Catalysts 11 (2021) 265, https://doi.org/10.3390/catal11020265.

[30] I.-W. Wang, D.A. Kutteri, B. Gao, H. Tian, J. Hu, Methane pyrolysis for carbon nanotubes and CO $_x$ -free H $_2$ over transition-metal catalysts, Energy Fuels 33 (2019) 197–205, https://doi.org/10.1021/acs.energyfuels.8b03502.

[31] M.v. Landau, N. Meiri, N. Utsis, R. Vidruk Nehemya, M. Herskowitz, Conversion of CO $_2$, CO, and H $_2$ in CO $_2$ hydrogenation to fungible liquid fuels on Fe-based catalysts, Ind. Eng. Chem. Res. 56 (2017) 13334–13355, https://doi.org/10.1021/acs.iecr.7b01817.

[32] X. Chen, X. Su, H. Duan, B. Liang, Y. Huang, T. Zhang, Catalytic performance of the Pt/TiO2 catalysts in reverse water gas shift reaction: controlled product selectivity and a mechanism study, Catal. Today 281 (2017) 312–318, https://doi.org/10.1016/j.cattod.2016.03.020.

[33] Q. Zhang, L. Pastor-Perez, Q. Wang, T. Ramirez Reina, Conversion of CO2 to added value products via RWGS using Fe-promoted catalysts: carbide, metallic Fe or a mixture? J. Energy Chem. 66 (2022) 635–646, https://doi.org/10.1016/j.jechem.2021.09.015.

[34] L. Wang, H. Liu, Y. Liu, Y. Chen, S. Yang, Influence of preparation method on performance of Ni-CeO2 catalysts for reverse water-gas shift reaction, J. Rare Earths 31 (2013) 559–564, https://doi.org/10.1016/S1002-0721(12)60320-2.

[35] B. Dai, S. Cao, H. Xie, G. Zhou, S. Chen, Reduction of CO2 to CO via reverse water-gas shift reaction over CeO2 catalyst, Kor. J. Chem. Eng. 35 (2018) 421–427, https://doi.org/10.1007/s11814-017-0267-y.

[36] Q. Zhang, L. Pastor-Perez, W. Jin, S. Gu, T.R. Reina, Understanding the promoter effect of Cu and Cs over highly effective β-Mo2C catalysts for the reverse water-gas shift reaction, Appl. Catal., B 244 (2019) 889–898, https://doi.org/10.1016/j.apcatb.2018.12.023.

[37] Y. Zhuang, R. Currie, K.B. McAuley, D.S.A. Simakov, Highly-selective CO2 conversion via reverse water gas shift reaction over the 0.5wt% Ru-promoted Cu/ZnO/Al2O3 catalyst, Appl. Catal. Gen. 575 (2019) 74–86, https://doi.org/10.1016/j.apcata.2019.02.016.

[38] B. Dai, G. Zhou, S. Ge, H. Xie, Z. Jiao, G. Zhang, K. Xiong, CO $_2$ reverse water-gas shift reaction on mesoporous M-CeO $_2$ catalysts, Can. J. Chem. Eng. 95 (2017) 634–642, https://doi.org/10.1002/cjce.22730.
[39] A. Ranjbar, A. Irankhah, S.F. Aghamiri, Reverse water gas shift reaction and CO2 mitigation: nanocrystalline MgO as a support for nickel based catalysts, J. Environ. Chem. Eng. 6 (2018) 4945–4952, https://doi.org/10.1016/j.jece.2018.07.032.
[40] L. Pastor-Perez, M. Shah, E. le Saché, T. Ramirez Reina, Improving Fe/Al2O3 catalysts for the reverse water-gas shift reaction: on the effect of Cs as activity/selectivity promoter, Catalysts 8 (2018) 608, https://doi.org/10.3390/catal8120608.